European Conference on Optical Communication (ECOC) 2022 © Optica Publishing Group 2022

Photonic Inverse Design of Compact Stokes-Vector Receivers on Commercial Foundry Platforms

Alec M. Hammond, C. Alex Kaylor, Joel Slaby, Michael Probst, Stephen E. Ralph*

School of Electrical & Computer Engineering, Georgia Institute of Technology, Atlanta, GA USA
*stephen.ralph@ece.gatech.edu

Abstract *We present and experimentally validate an ultra-compact, silicon-photonics, Stokes-vector receiver designed entirely using topology optimization. The system occupies just 0.06 mm^2 and is amenable to optical/electrical flip-chip packaging. Experiments demonstrate a median error angle of 14° without tuning across the Poincaré sphere and optical C-band. ©2022 The Author(s)*

Introduction

Ongoing interest in Telecom, Datacom, and NewSpace infrastructure motivates a low-cost, high-density communications platform that achieves the performance and flexibility of coherent systems without sacrificing the simplicity and efficiency of direct detection. Stokes-vector receivers (SVR) aim to maximize the benefits of both these paradigms by encoding in (3D) Stokes space[1], a high-density, direct-detect format compatible with many field-recovery algorithms[2]. Furthermore, these receivers are needed for various polarimetry, test and measurement, and sensing applications. Despite various successful demonstrations on different integrated platforms[3]–[9], realizing a compact, robust architecture compatible with a "turn-key" silicon photonics foundry remains a longstanding challenge.

We present and experimentally validate an ultra-compact, silicon photonics SVR designed entirely using density-based topology optimization (TO). To our knowledge, this is the first inverse-designed, high-density communications system fabricated and tested on a commercial-foundry, silicon-photonics platform. The system consists of single- and dual-polarization grating couplers, a 90° hybrid, and a 33/66 splitter. Notably, each component was optimized to adhere to thousands of design rule checks (DRC) without requiring any additional post-processing (or DRC waivers)[10]. The system was fabricated on the (300 mm) GlobalFoundries 45CLO silicon photonics CMOS process leveraging both the standard silicon-on-insulator (SOI) and polysilicon layers[11]. It occupies a compact footprint of 0.06 mm^2 (including optical IO), interfaces with standard vertical fiber arrays (0° to the normal), and therefore is amenable to optical/electrical flip-chip packaging. Future iterations incorporating integrated photodiodes further consolidate the final footprint. Experiments demonstrate a median error angle of 14° across the entire Poincaré sphere and optical C-band.

Our system is orders of magnitude smaller than the current state of the art, but leverages generalizable, inverse-designed components that can be readily implemented in other photonic circuits (e.g. coherent receivers, polarimeters, Lidar, etc.). In addition, our methodology extends itself to arbitrary foundries and material platforms, paving the way toward an "architecture-first" design flow, where robust device-design is no longer the bottleneck for integrated photonic system design. Indeed, while traditional (intuition-first) design methodologies often encounter tradeoffs between packaging complexity, system size, or device efficiency, our work indicates that TO thrives in highly constrained problem spaces (as demonstrated by the compact, high-efficiency, 0° dual-polarization grating coupler) enabling a new generation of photonic system design.

System design and operation

We designed each component of the integrated SVR using our density-based topology optimization toolbox[12],[13], which uniquely enables large-scale, multi-layer, photonic inverse design. Using this approach, the design is parameterized by thousands of individual "pixels" which freely evolve between the core and cladding materials until the user-specified figure of merit (FOM) is satisfied[14],[15]. A hybrid time-/frequency-domain adjoint-variable method (AVM)[16] is employed to efficiently compute broadband gradients w.r.t. all degrees of freedom using just two fullwave Maxwell solves. We designed broadband, multi-layer, single- and dual-polarization grating cou-

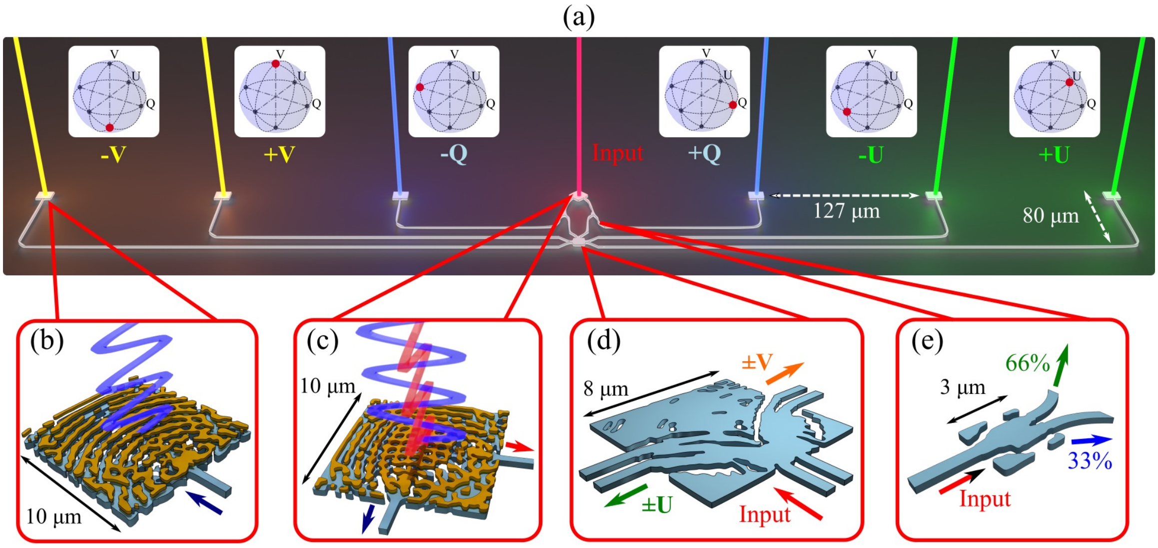

Fig. 1: Inverse-designed Stokes receiver architecture (a). A dual-polarization grating coupler (c) receives the input signal (red), demultiplexing each (linear) polarization state from the fiber into a 33/66 asymmetric splitter (e). The splitter sends 33% of each polarization directly to a single-polarization grating coupler (b), which corresponds to linear polarization states $\pm\boldsymbol{Q}$ (blue). The remaining 66% is routed to a 90° hybrid (d), which interferes both polarization states in order to decode the $\pm\boldsymbol{V}$ (yellow) and $\pm\boldsymbol{U}$ (green) Stokes vectors. Each respective polarization state is depicted on the Poincaré sphere alongside each output port.

plers, an asymmetric 33/66 splitter, and an interferometrically robust 90° hybrid. We employed specialized optimization constraints to ensure the final devices would adhere to thousands of design rule checks[10], like minimum linewidth, linespacing, area, enclosed area, and curvature. The final inverse-designed devices were strategically cascaded to form the final SVR architecture. Fig. 1 describes the SVR architecture, its operation, and each constituent inverse-designed component. The architecture itself takes an input polarization symbol and decodes it into the Stokes basis states ($\pm\boldsymbol{U}$, $\pm\boldsymbol{V}$, and $\pm\boldsymbol{Q}$). Three balanced detectors, one on the output of each basis vector, provides the final measured symbol in Stokes space. In this iteration, optical outputs provide direct access to device characteristics, but future iterations will include integrated photodiodes.

Experimental results

We coupled light into the integrated SVR's TO-designed grating couplers using index-matching fluid (ThorLabs) and a standard SMF-28 fiber array (OZ Optics) with 127 µm pitch. A continuous wave (CW) optical signal was generated using a Keysight 81642A swept-source laser and modulated using a Keysight N7786B polarization synthesizer, which dynamically tunes the input optical signal to any arbitrary point on the Poincaré sphere's surface. The six optical outputs were detected using logarithmic (high dynamic range) photodiodes (Newport and Koheron).

To characterize the SVR, we sent and received 184 symbols evenly spaced in the azimuthal (linear polarization state) and elliptical directions. Fig. 2 depicts the sent and received symbols at 1550 nm. To calibrate each measurement, we prepended to each sequence the six components of the fundamental Stokes basis, which we used to estimate the affine transformation using a least-squares regression. We repeated this experiment for eleven distinct wavelengths from 1530 nm to 1580 nm, and characterized the error using the angular distance between sent and received symbols. Fig. 3 describes the symbol error angle in degrees as a function of azimuthal and elliptical angle at 1550 nm.

To better understand the system response, we individually characterized the polarization diversity and phase response of each component. We determined the primary source of distortion is likely due to the relative phase ($\pm$ 8°) and magnitude ($\pm$ 5%) deviations of the 90° hybrid. New design iterations demonstrate improved phase tolerance. The logarithmic detectors also contributed to symbol skew. Our next-generation system will include monolithically integrated balanced detectors and high-speed transimpedance amplifiers. Our current iteration demonstrates useful performance at a significantly smaller scale than previously reported. Furthermore, the constituent components of the SVR provide fundamental building blocks that can be used to implement other systems on the same platform.

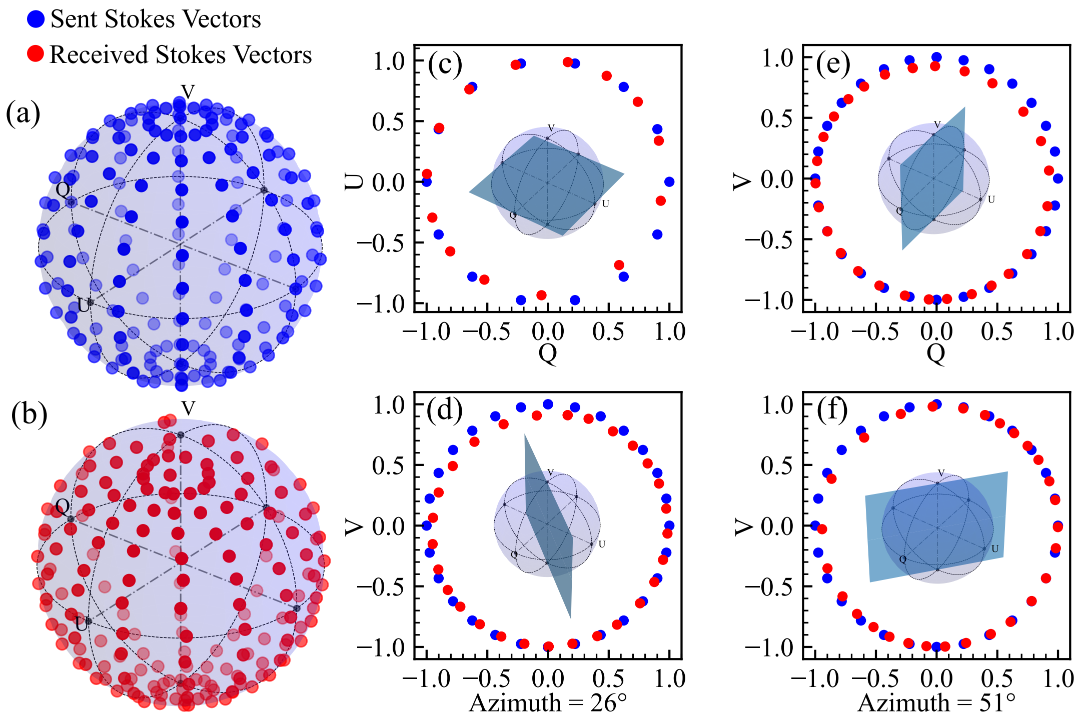

Fig. 2: Experimental performance of the inverse-designed SVR. (a) and (b) show the sent and received Stokes vectors, respectively, on the Poincaré Sphere at 1550 nm. (c)-(f) show planar slices of the received constellations. Independent experimental measurements of the individual polarization grating couplers revealed >30 dB of polarization extinction across the band. In contrast, isolated experimental characterization of the 90° hybrid revealed an 8° phase deviation in one of the output arms, which is consistent with the observed symbol distortion near $+\boldsymbol{V}$ (b).

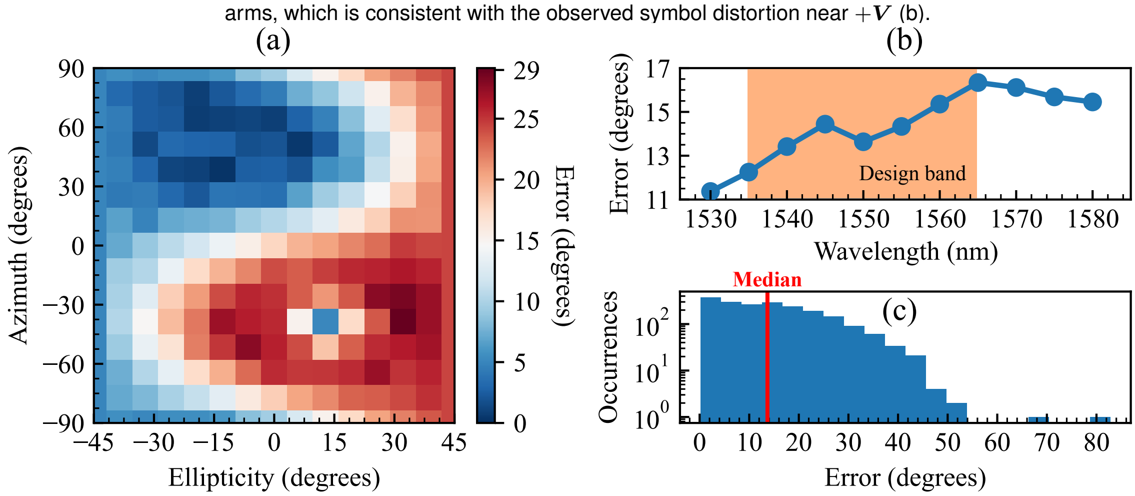

Fig. 3: SVR system characterization. Errors across the Poincaré Sphere at 1550 nm (a) show a division between equal-area low- and high-error regions that is likely due to the non-ideal phase/magnitude response of the 90° hybrid and the logarithmic response of the photodetectors (requiring extra calibration). The minimum error is 0.33° while the maximum is 29.16°. The median errors across a wide band (b) show increasing error towards longer wavelengths, but still demonstrate acceptable performance outside of the design band. The distribution of errors created by aggregating all the wavelength data (c). Assuming an error threshold of 28°, 16 equidistant symbols along the surface of the sphere can be reliably decoded (in a noise-free environment) corresponding to a 4-bit transmission system (or PAM-4 along two axes). Additionally modulating the amplitude of each symbol will further increase the spectral efficiency of the SVR.

Acknowledgements

The authors thank GlobalFoundries for silicon fabrication through the 45CLO university program, as well as the Partnership for an Advanced Computing Environment (PACE) at Georgia Tech for providing computational resources. AMH was supported by the National Defense Science & Engineering Graduate (NDSEG) Fellowship Program. This work continues under the NSF-IUCRC EPICA center Grant No. 2052808.

References

[1] X. Chen, C. Antonelli, D. Mecozzi Antonio Che, and W. Shieh, “High-capacity direct-detection systems”, in *Optical Fiber Telecommunications VII*, Academic Press, 2019, pp. 419–441.

[2] D. Che, C. Sun, and W. Shieh, “Optical field recovery in stokes space”, *Journal of Lightwave Technology*, vol. 37, no. 2, pp. 451–460, 2019.

[3] T. Suganuma, W. Yanwachirakul, E. Kato, M. Sugiyama, Y. Nakano, and T. Tanemura, “Fully integrated 4-port stokes vector receiver for multi-level 3d signal detection”, in *2019 24th OptoElectronics and Communications Conference (OECC) and 2019 International Conference on Photonics in Switching and Computing (PSC)*, IEEE, 2019, pp. 1–3.

[4] A. M. Hammond and S. E. Ralph, “System-level inverse design for stokes receivers on a commercial foundry platform”, in *Optical Fiber Communication Conference*, Optical Society of America, 2021, W6A–5.

[5] S. Ghosh, Y. Kawabata, T. Tanemura, and Y. Nakano, “Polarization-analyzing circuit on inp for integrated stokes vector receiver”, *Opt. Express*, vol. 25, no. 11, pp. 12 303–12 310, 2017.

[6] M. Baier, F. M. Soares, A. Schoenau, *et al.*, “Fully integrated stokes vector receiver for 400 gbit/s”, in *2019 Optical Fiber Communications Conference and Exhibition (OFC)*, IEEE, 2019, pp. 1–3.

[7] Z. Lin, L. Rusch, Y. Chen, and W. Shi, “Chip-scale, full-stokes polarimeter”, *Opt. Express*, vol. 27, no. 4, pp. 4867–4877, 2019.

[8] C. Zhou, Y. Xie, J. Ren, *et al.*, “Spin separation based on-chip optical polarimeter via inverse design”, *Nanophotonics*, vol. 11, no. 4, pp. 813–819, 2022.

[9] P. Dong, X. Chen, K. Kim, S. Chandrasekhar, Y.-K. Chen, and J. H. Sinsky, “128-gb/s 100-km transmission with direct detection using silicon photonic stokes vector receiver and I/Q modulator”, *Opt. Express*, vol. 24, no. 13, pp. 14 208–14 214, 2016.

[10] A. M. Hammond, A. Oskooi, S. G. Johnson, and S. E. Ralph, “Photonic topology optimization with semiconductor-foundry design-rule constraints”, *Opt. Express*, vol. 29, no. 15, pp. 23 916–23 938, 2021.

[11] K. Giewont, K. Nummy, F. A. Anderson, *et al.*, “300-mm monolithic silicon photonics foundry technology”, *IEEE Journal of Selected Topics in Quantum Electronics*, vol. 25, no. 5, pp. 1–11, 2019.

[12] A. M. Hammond, A. Oskooi, M. Chen, Z. Lin, S. G. Johnson, and S. E. Ralph, “High-performance hybrid time/frequency-domain topology optimization for large-scale photonics inverse design”, *Opt. Express*, vol. 30, no. 3, pp. 4467–4491, 2022.

[13] A. F. Oskooi, D. Roundy, M. Ibanescu, P. Bermel, J. D. Joannopoulos, and S. G. Johnson, “MEEP: A flexible free-software package for electromagnetic simulations by the FDTD method”, *Computer Physics Communications*, vol. 181, no. 3, pp. 687–702, 2010.

[14] O. Sigmund and K. Maute, “Topology optimization approaches”, *Structural and Multidisciplinary Optimization*, vol. 48, no. 6, pp. 1031–1055, 2013.

[15] S. Molesky, Z. Lin, A. Y. Piggott, W. Jin, J. Vucković, and A. W. Rodriguez, “Inverse design in nanophotonics”, *Nature Photonics*, vol. 12, no. 11, pp. 659–670, Oct. 2018.

[16] G. Strang, *Computational Science and Engineering*. Wellesley, MA: Wellesley-Cambridge Press, 2007.